lubricants

MDPI

Article

Enhancing Machining Efficiency: Real-Time Monitoring of Tool Wear with Acoustic Emission and STFT Techniques

Luís Henrique Andrade Maia [1,*], Alexandre Mendes Abrão [2], Wander Luiz Vasconcelos [3], Jánes Landre Júnior [1], Gustavo Henrique Nazareno Fernandes [1] and Álisson Rocha Machado [4,5]

[1] Graduate Program in Mechanical Engineering, Pontifical Catholic University of Minas Gerais—PUC Minas, Belo Horizonte 30535-901, MG, Brazil; janes@gmail.com (J.L.J.); ghnfernandes@gmail.com (G.H.N.F.)
[2] Graduate Program in Mechanical Engineering, Federal University of Minas Gerais—UFMG, Belo Horizonte 31270-901, MG, Brazil; abrao@demec.ufmg.br
[3] Graduate Program in Metallurgical and Materials Engineering, Federal University of Minas Gerais—UFMG, Belo Horizonte 31270-901, MG, Brazil; wlv@demet.ufmg.br
[4] Faculty of Mechanical Engineering—FEMEC, Federal University of Uberlândia—UFU, Uberlândia 38408-100, MG, Brazil; alissonr.machado@gmail.com
[5] Mechanical Engineering Graduate Program, Pontifícia Universidade Católica do Paraná—PUCPR, Rua Imaculada, Conceição, 1155, Prado Velho, Curitiba 80215-901, PR, Brazil
* Correspondence: luismaia@pucminas.br

Abstract: Tool wear in machining is inevitable, and determining the precise moment to change the tool is challenging, as the tool transitions from the steady wear phase to the rapid wear phase, where wear accelerates significantly. If the tool is not replaced correctly, it can result in poor machining performance. On the other hand, changing the tool too early can lead to unnecessary downtime and increased tooling costs. This makes it critical to closely monitor tool wear and utilize predictive maintenance strategies, such as tool condition monitoring systems, to optimize tool life and maintain machining efficiency. Acoustic emission (AE) is a widely used technique for indirect monitoring. This study investigated the use of Short-Time Fourier Transform (STFT) for real-time monitoring of tool wear in machining AISI 4340 steel using carbide tools. The research aimed to identify specific wear mechanisms, such as abrasive and adhesive ones, through AE signals, providing deeper insights into the temporal evolution of these phenomena. Machining tests were conducted at various cutting speeds, feed rates, and depths of cut, utilizing uncoated and AlCrN-coated carbide tools. AE signals were acquired and analyzed using STFT to isolate wear-related signals from those associated with material deformation. The results showed that STFT effectively identified key frequencies related to wear, such as abrasive between 200 and 1000 kHz and crack propagation between 350 and 550 kHz, enabling a precise characterization of wear mechanisms. Comparative analysis of uncoated and coated tools revealed that AlCrN coatings reduced tool wear extending tool life, demonstrating superior performance in severe cutting conditions. The findings highlight the potential of STFT as a robust tool for monitoring tool wear in machining operations, offering valuable information to optimize tool maintenance and enhance machining efficiency.

Keywords: acoustic emission; short-time fourier transform; wear mechanisms; turning; AISI 4340

Citation: Maia, L.H.A.; Abrão, A.M.; Vasconcelos, W.L.; Júnior, J.L.; Fernandes, G.H.N.; Machado, Á.R. Enhancing Machining Efficiency: Real-Time Monitoring of Tool Wear with Acoustic Emission and STFT Techniques. *Lubricants* **2024**, *12*, 380. https://doi.org/10.3390/lubricants12110380

Received: 6 September 2024
Revised: 12 October 2024
Accepted: 28 October 2024
Published: 31 October 2024

1. Introduction

Tool wear in machining is inevitable [1–4]. The characteristic life curve of a cutting tool typically progresses through three stages. The initial stage involves accelerated wear, primarily influenced by the tribological behavior of the system. During this break-in period, contact between the tool and workpiece occurs primarily at the asperities of both surfaces [5]. This results in stress concentration over a small area, leading to significant shear forces and, consequently, pronounced initial wear.

The second stage is characterized by a period of steady or uniform wear. In this phase, the tool's wear rate stabilizes as the contact surface between the tool and workpiece becomes smoother and more consistent. The tribological system reaches a balance, where the rate of material removal from the tool is relatively constant, allowing the tool to perform predictably and efficiently over an extended period. This is typically the longest phase of the tool's life, during which the cutting performance remains reliable and within acceptable limits [6].

The problem lies at the interface between the second and third stages, where determining the precise moment to change the tool becomes a challenge. The tool transitions from the steady wear phase to the rapid wear phase accelerate significantly, leading to a sharp decline in cutting performance and an increased risk of tool failure. If the tool is not replaced at the right time, it can result in poor surface finish, dimensional inaccuracies, and even catastrophic tool breakage, potentially damaging the workpiece and the machine. On the other hand, changing the tool too early can lead to unnecessary downtime and increased tooling costs. This makes it critical to monitor the tool closely and utilize predictive maintenance strategies, such as tool condition monitoring systems, to optimize tool life and maintain machining efficiency [7].

Acoustic emission (AE) is a widely used technique for indirect monitoring, particularly in the context of static equipment and pressurized vessels [8–10]. This technique refers to the energy released by a material when its structure is altered, such as during corrosion, deformation, wear, or shearing. This energy is detected as transient elastic waves, which can be analyzed to monitor the condition of the material [11]. However, the application of AE in cutting processes presents challenges due to the complexity of the mechanisms involved, especially the signal processing [12].

The Short-Time Fourier Transform (STFT) is a widely used signal processing technique that enables time-frequency analysis of non-stationary signals. It divides the signal into smaller, overlapping time windows, applying the Fourier Transform to each segment to produce a representation of how the frequency content evolves over time [13]. Unlike the Fast Fourier Transform (FFT), which only offers a global frequency overview, STFT captures both temporal and spectral information, making it ideal for analyzing transient signals, such as those found in acoustic emissions and speech [14]. However, STFT has an inherent trade-off: smaller time windows offer better temporal resolution but sacrifice frequency precision, and larger windows provide higher frequency resolution but lower time accuracy [15].

Other time-frequency methods, such as the Wavelet Transform (WT) and Hilbert–Huang Transform (HHT), provide alternatives to STFT. WT offers adaptive time-frequency resolution, allowing for the analysis of signals with varying frequency characteristics [16]. HHT is particularly effective for analyzing non-linear and non-stationary signals by decomposing the signal into intrinsic mode functions, offering a more refined view of time-frequency dynamics compared to STFT [17]. The following Table 1 compares the key features of STFT, FFT, WT, and HHT:

Table 1. The key features of STFT, FFT, WT.

Technique	Time Resolution	Frequency Resolution	Application	Strengths	Weaknesses
STFT	Medium (depends on window size)	Medium (depends on window size)	Transient signals in machining, speech, etc.	Provides localized time-frequency analysis	Time-frequency trade-off due to fixed window size
FFT	None (global analysis)	High	Periodic, stationary signals	Efficient for stationary signals with high frequency accuracy	No time information

Table 1. *Cont.*

Technique	Time Resolution	Frequency Resolution	Application	Strengths	Weaknesses
Wavelet Transform	Adaptive	Adaptive	Non-stationary signals, medical, engineering	Flexible, multi-resolution analysis of complex signals	Computationally more expensive
Hilbert–Huang Transform	High	High	Non-linear, non-stationary signals	Ideal for analyzing non-linear and non-stationary signals	Complex implementation and interpretation

Several cutting-related phenomena, such as dislocation movement, void coalescence, and twin formation, generate acoustic emissions at various frequencies; however, these frequencies are not well defined [18]. Additionally, the effects of temperature, wear, and friction at the chip-tool-workpiece interfaces further complicate the interpretation of AE signals. Understanding and isolating these contributing factors is essential for the effective application of AE in machining operations [19].

The basic premise of acoustic emission (AE) in tribological friction is that when two surfaces are in contact, various macro and micro processes contribute to structural changes. These processes include plastic deformation, micro and macrocrack formation and propagation, phase transformations, adhesive bond formation and destruction, as well as corrosion and oxidation. All of these physico–mechanical and chemical–mechanical processes generate acoustic emission [20–22]. To accurately interpret AE signals in tribological processes, it is crucial to understand how the elastic interactions of surface roughness are translated into AE signals. This understanding allows for the differentiation or elimination of signals generated by wear mechanisms from those produced by surface interactions [23].

When two contact surfaces experience displacement and friction, acoustic emission (AE) signals tend to oscillate slightly. The tribological profile of the contact pair evolves due to factors such as heating, oxide formation, and changes in the stress state. The broad frequency range of AE signals (10 kHZ to 1.6 MHz) can lead to difficulties in accurately identifying specific events, potentially masking various phenomena and resulting in erroneous conclusions [24]. A deeper understanding of the specific frequency ranges associated with different events, combined with precise boundary conditions, would enhance the accuracy of AE signal interpretation, leading to more reliable and meaningful conclusions [25].

For example, Hase et al. [26] investigated the characteristics of acoustic emission (AE) signals and their correlation with various phenomena, including different wear mechanisms. Abrasive wear spans a broad frequency range (200 kHz to 1 MHz), with well-defined peaks that can help identify the dominant wear mechanism in an experiment. Crack propagation typically generates AE signals within the range of 100 to 700 kHz, overlapping with the frequencies produced by abrasive wear. Slip excitation is found in a narrower band (25 to 110 kHz) and overlaps with signals from mild adhesive wear and particle interactions. Other wear mechanisms exhibit distinct peaks and produce much lower-frequency bands compared to abrasive wear.

Lu et al. [27] studied the efficacy of the STFT, wavelet, and Hilbert–Huang transform for the analysis of AE signals in the carbon fiber compression test. To this end, the authors imposed a compression speed on a specimen measuring 100 mm × 20 mm × 2.5 mm. The authors stated that the STFT and the wavelet did not adjust to the point of causing a variation in the excitation in terms of time and frequency (known as pitching). However, the Hilbert–Huang transform was more effective for monitoring in the test. They further concluded that the fracture of the carbon fiber generated excitation at a frequency of 275 kHz while the cracks in the matrix generated excitations in the frequency range of 175 to 200 kHz.

Marinescu and Axinte [28] used the STFT technique to detect failures in mill-machined parts with multiple cutting edges simultaneously. The authors milled Inconel 718 with five carbide inserts coated with TiAlN + TiN. The tests were performed varying the radial depth of cut so that the number of cutting edges in contact with the workpiece varied, while changing the axial depth of cut so that it generated practically the same signal amplitudes. The AE signals demonstrated by STFT were extremely sensitive to the excitation variation generated by the number of sharp edges during cutting. The authors also generated a defective surface by imposing an insert with sharp wear on the tool and analyzed the STFT of the operation. They concluded that with the use of the technique to monitor the milling process, failures in the machined parts could be identified.

Maia et al. [8] developed a new technique to monitor tool wear using AE signals and to determine the tool life in machining with carbide inserts. A high-pass filter was used and the filtered signal, along with the amplitude of the modulated signal, was combined. So, the auto covariance was represented by the power spectral density (PSD) technique. The technique was found to be very sensitive to the level of wear of the tool, in addition to detecting the mechanisms involved. A significant difference is that, in the study reported herein, only the filtered signals were considered, and these were processed using the STFT technique, which shows the temporal variation of the frequencies and confirms that the mechanisms of wear act discretely on the tool over time.

In this study, we aim to address the existing gap in understanding the wear mechanisms during the turning of AISI 4340 steel with cemented carbide tools by employing the Short-Time Fourier Transform (STFT) technique to analyze acoustic emission (AE) signals. Despite previous studies on tool wear monitoring, the complexity and interplay of various wear mechanisms during machining have not been fully elucidated, particularly in real-time analysis. The novelty of this research lies in the application of STFT to isolate and identify specific wear mechanisms such as abrasive and adhesive, as well as their temporal evolution. By providing a more precise characterization of these mechanisms, this study not only helps to advance the fundamental knowledge in the field of machining but also offers practical insights into optimizing tool life and improving machining performance.

2. Methodology

The material chosen was the AISI 4340 due to its applicability. It is a low-alloy steel known for its exceptional toughness, strength, and wear resistance. It contains significant amounts of nickel, chromium, and molybdenum, which contribute to its high hardenability and mechanical properties, even in large sections. The typical composition includes 0.38–0.43% carbon, 0.70–0.90% chromium, 1.65–2.00% nickel, 0.20–0.30% molybdenum, and a balance of iron. This alloy is widely used in applications that require high strength and fatigue resistance, such as aircraft landing gear, crankshafts, and other critical components subjected to heavy loads. AISI 4340 can be heat treated to enhance its mechanical properties, achieving high tensile strength, excellent toughness, and good ductility. Its combination of hardness and toughness makes it ideal for demanding industrial applications, including aerospace, automotive, and heavy machinery. Additionally, it exhibits poor machinability. It can maintain mechanical properties even at elevated temperatures. The AISI 4340 steel workpieces used in this study have a hardness of 46 $\pm$ 1 HRC (474 HV) and were 300 mm in length with a diameter of 70 mm, machined in two passes of 150 mm each. Table 2 presents some properties of the AISI 4340 [29].

Micrographs of the samples (Figure 1) reveal the presence of ferrite, martensite, and carbides in the darker regions (grey and black). Ferrite, which is softer and more ductile, typically appears as lighter areas in AISI 4340 steel, identifiable by its smooth, equiaxed grain structure. Martensite, on the other hand, is characterized by its needle-like or lath structure, which appears darker and more irregular due to its brittleness and higher hardness formed by rapid cooling. Carbides are present as even darker particles, enhancing wear resistance and contributing to the hardness of the material.

Table 2. Properties of the AISI 4340.

Property	AISI 4340	Element	Composition (%)
Necking (%)	33.3	Carbon (C)	0.38–0.43
Elongation (%)	13	Chromium (Cr)	0.70–0.90
Yield Strength (MPa)	1672	Manganese (Mn)	0.60–0.80
Ultimate Tensile Strength (MPa)	2028	Nickel (Ni)	1.65–2.00
Elastic Modulus (GPa)	200–210	Molybdenum (Mo)	0.20–0.30
Hardness (Vickers HV)	474	Silicon (Si)	0.15–0.30
Density (g/cm^3)	7.85	Sulfur (S)	Max 0.040
Melting Point (°C)	1425–1450	Phosphorus (P)	Max 0.035
Thermal Conductivity (W/m·K)	44–48	Iron (Fe)	Balance

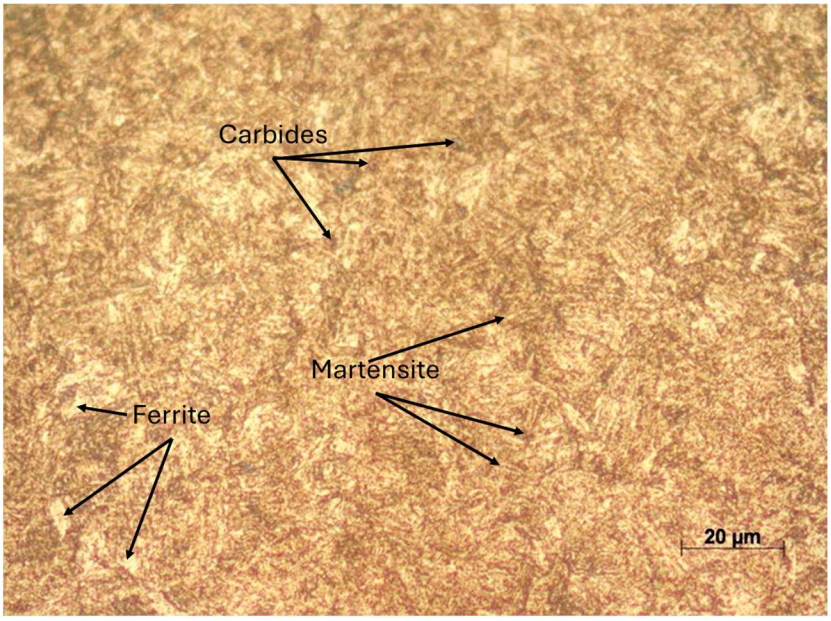

Figure 1. Micrograph of the quenched AISI 4340 steel.

Given the extreme sensitivity of AE signals acquired during machining to various excitations—including deformation and defect movement mechanisms—preliminary tensile tests were conducted on the steel. These tests aimed to monitor and differentiate the AE signals originating from deformation processes and those related to tool wear mechanisms during machining. The tensile tests were performed with a claw displacement velocity (deformation rate) of 2 mm/s, chosen to allow detection of isolated events generated by the phenomena responsible for steel excitation. The tests were monitored using an acoustic emission (AE) sensor fixed to the useful length of the specimen, with AE data acquired from the onset of elastic deformation to specimen rupture.

Deformation curves for AISI 4340 steel were obtained using a universal testing machine, the EMIC DL 20000MF, which has a maximum load capacity of 200 kN. This machine operates on a single-phase electromechanical system driven by a variable speed motor and ball screw, enabling testing speeds ranging from 0.01 mm/min to 50 mm/min. Force measurements were carried out using load cells in compliance with the ISO 7500-1 standard [30], while displacement was measured with an optical sensor boasting a resolution of 0.01 mm and a maximum stroke length of 220 mm. The machine's instrumentation, integrated into its cabinet, was designed to operate in conjunction with a microcomputer, ensuring precise data acquisition. Figure 2 demonstrate results from the tensile tests for the AISI 4340.

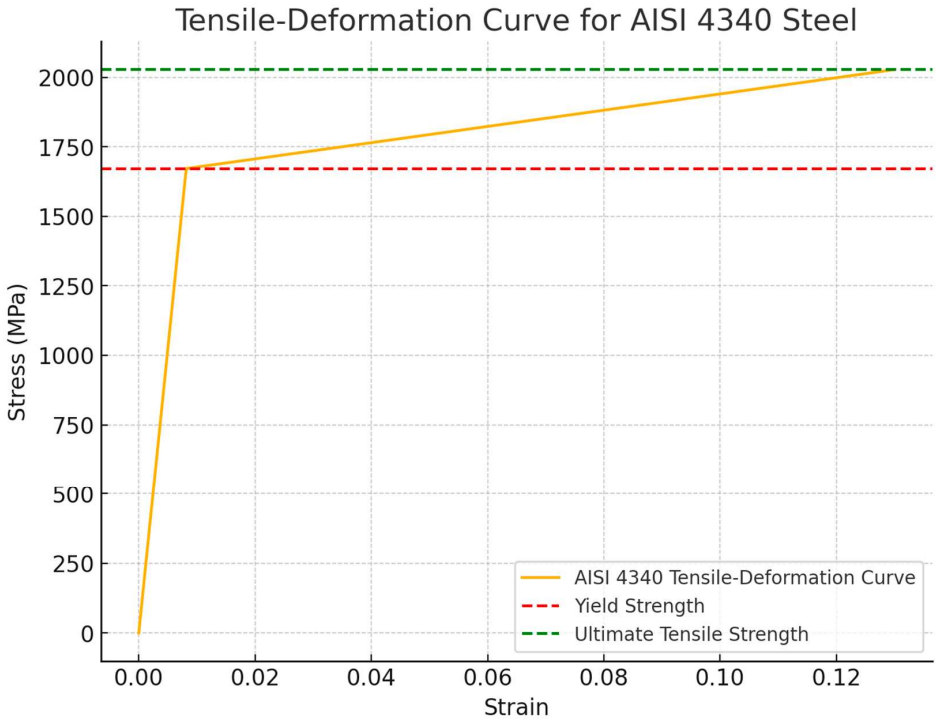

Figure 2. Sketch of the tensile test curve for AISI 4340 steel.

Turning tests were performed on a Centur CNC lathe (model 30D), manufactured by Indústrias ROMI S.A (Santa Bárbara d'Oeste, Brazil). This lathe, with a power output of 7.5 kW, features a variable spindle speed range from 4 to 4000 rpm, a maximum permissible diameter of 200 mm, and a maximum workpiece length of 1000 mm. The machine's numerical control system is the MACH 9.

Cemented carbide inserts with the ISO designation SNMA 120408 K10-20 grade, without a chip breaker, ISCAR brand were utilized. These inserts were mounted on an ISCAR toolholder, ISO code DSBNR 2525 M12. Although K-grade cemented carbide is typically recommended for turning cast iron, this grade was selected due to its accelerated wear behavior when turning steels. A sample of the inserts was sent to Oerlikon Balzers to be coated. Some inserts received a monolayer of AlCrN, as Figure 3, while others were coated with a nanostructured AlCrN layer, both applied by PVD with a thickness of 4 µm. Uncoated inserts were retained as control samples.

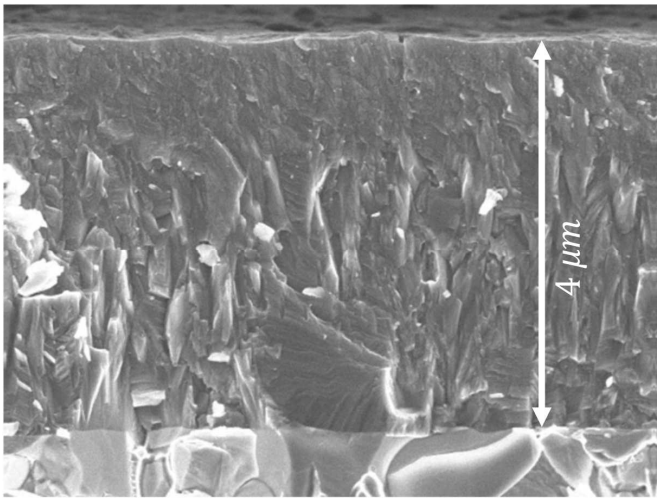

Figure 3. Side-cut view of AlCrN coating with thickness of 4 µm on hard metal substrate [31].

AlCrN coatings, commonly deposited using PVD techniques, typically range in thickness from 1 to 5 µm, with a microhardness of approximately 1900 HV and an oxidation temperature above 700 °C. This coating offers moderate thermal barrier properties, abrasion resistance, adhesion wear resistance, diffusion wear resistance, and substrate protection against corrosion [31,32]. Table 3 presents some properties.

Table 3. Some properties of the AlCrN coating.

Structure	AlCrN
Hardness (HV 0.05)	3200
Residual stresses (GPa)	−3.0
Maximum service temperature (°C)	1100
Coefficient of friction (*CoF*)	0.3
Carbide applications (milling/finishing)	• *Steels* > 1000 N/mm^2 • *Steels* > 45 ∼ 52 HRC • Stainless steel • Grey cast iron • Titanium and its alloys • Inconel
HSS applications (milling/finishing)	• Stainless steel • Grey cast iron • Titanium and its alloys

Table 3 AlCrN coating specifications [31].

For acoustic emission data acquisition, a physical acoustic piezoelectric transducer model R15i was employed along with a Spartan 2000 signal conditioner. The signals were acquired using a National Instruments PCI-6251 card (National Instruments, Austin, TX, USA), capable of a maximum acquisition rate of 1.2 MS/s. The sensor, measuring 20.6 mm in diameter and 27 mm in height, was positioned on the specimen during tensile tests and on the tool holder during turning tests. Figures 4 and 5 illustrate the data acquisition diagrams for both test types and the frequency response curve of the R15i sensor.

The AE sensor was validated using a graphite-breaking test, which demonstrates the sensor's sensitivity and the excited frequency spectrum. This method is recommended by the sensor manufacturer to ensure proper sensor validation. Figure 5 shows the frequency response of the sensor used in the tests.

The AE sensor was validated using a graphite-breaking test, as recommended by the sensor manufacturer, to assess the sensor's sensitivity and accuracy in capturing the frequency spectrum. Figure 5 illustrates the sensor's frequency response, which exhibits fluctuations across the 0 to 1 MHz range. These fluctuations indicate the varying sensitivity of the sensor at different frequencies, with peaks observed around 0.2 MHz and smaller fluctuations between 0.6 and 1 MHz. The higher sensitivity at lower frequencies is consistent with the expected performance of the R15i sensor, as its design is optimized for detecting lower-frequency acoustic emissions typical in machining operations. The dips in the response, particularly after 0.6 MHz, reflect the reduced sensor sensitivity at higher frequencies, which can be attributed to the specific characteristics of the piezoelectric material and the test setup used for validation. This validated frequency response ensures that the sensor accurately captures the AE signals associated with wear mechanisms during the machining process.

Tool wear was measured using a Mitutoyo TM 15 optical stereomicroscope (Mitutoyo America Corporation, Kanagawa, Japan) with a micrometric screw resolution of 1 µm and a magnification of 15×. The tool life criterion was based on ISO 3685, considering an admissible flank wear of VBB ≥ 0.3 mm [33].

Turning tests were conducted under the following conditions: cutting speeds (vc) of 150 m/min, 200 m/min, and 250 m/min; feed rates (f) of 0.10 mm/rev and 0.20 mm/rev;

and depths of cut (ap) of 0.25 mm and 0.75 mm, all performed dry and without chip breakers. These parameters were selected to reflect typical conditions used with carbide tools in industrial settings.

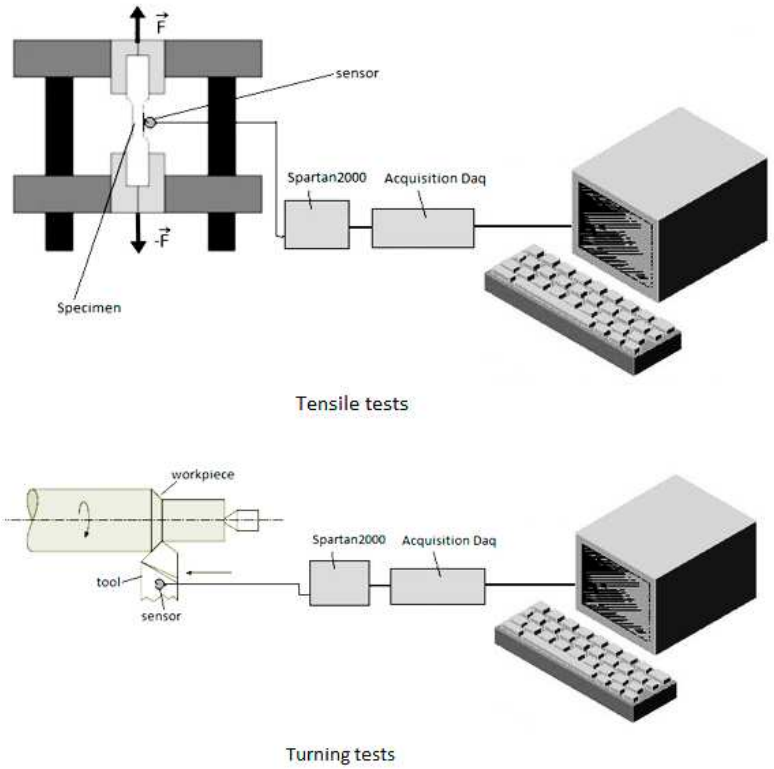

Figure 4. AE sensor fixation diagram for tensile and turning tests.

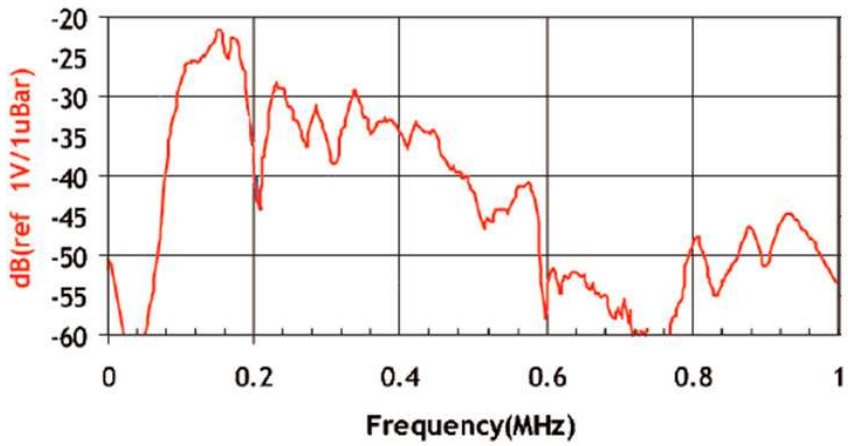

Figure 5. Frequency response of the AE R15i sensor.

AE signals were collected using a piezoelectric sensor fixed to the toolholder with petroleum jelly to enhance signal transmission, and data acquisition software developed on the LabVIEW platform. The acquisition rate was set at 400 kHz to manage data volume, with a 10 kHz active Butterworth high-pass filter applied to exclude non-excitatory signals. During turning tests, AE signals were collected for 2 s at the start and middle of the pass at a rate of 1.2 MHz (limited by the data acquisition board and the R15i sensor), using the same 10 kHz high-pass filter. Background noise signals were collected before testing to serve as a reference for noise elimination in the collected data using a suppressor filter.

To analyze the wear mechanisms visually, the tools were immersed in a 30% hydrochloric acid solution for 12 h to remove adhered work material. AISI 4340 steel turning tests were also performed to characterize the machining signals and compare them with the

tensile test signals, using the same three tools detailed earlier. The spectra obtained from the tensile and turning tests were compared, and the primary frequencies from each were separated. Deformation and fracture frequencies from the steel were used to create a filter to eliminate signals from the cutting process, isolating those originating from the tool.

The AE data were processed using custom software developed for this study and compared with results from other evaluated parameters. After each pass, the tool's flank wear was measured and analyzed using a stereomicroscope. Since the study's focus was not on establishing a tool life determination technique, as this was conducted in another study by Maia et al. [8], but rather on demonstrating the variation of excited frequencies over time, only the signals from the beginning and end of the tool's life were compared. Table 4 summarizes all the experimental conditions used.

Table 4. Experimental conditions condensed.

Experimental Condition	Details
Tool	Cemented carbide inserts, ISO SNMA 120408 K10-20 grade
Tool Coatings	Monolayer AlCrN, Nanostructured AlCrN (PVD, 3 μm)
Tool Life Criterion	Admissible flank wear VBB $\geq$ 0.3 mm (ISO 3685)
Microscope	Mitutoyo TM 15, 1 μm resolution, 15× magnification
Tensile Test Parameters	Claw displacement velocity: 2 mm/s
Turning Test Parameters	
-Cutting Speeds (vc)	150 m/min, 200 m/min, 250 m/min
-Feed Rates (f)	0.10 mm/rev, 0.20 mm/rev
-Depths of Cut (ap)	0.25 mm, 0.75 mm
Turning Conditions	Dry machining, no chip breakers
AE Sensor	R15i Piezoelectric sensor, fixed with petroleum jelly
Data Acquisition	
-Platform	LabVIEW
-Rate	400 kHz (regular acquisition), 1.2 MHz (specific tests)
-Filter	Active Butterworth high-pass filter at 10 kHz
Wear Mechanism Analysis	Tools immersed in 30% HCl solution for 12 h
Comparison Tests	AISI 4340 steel, tensile and turning tests
Noise Reduction	Background noise signals collected and filtered

The proposed method goes beyond traditional monitoring techniques by integrating the Short-Time Fourier Transform (STFT) to analyze acoustic emission (AE) signals during machining processes. Unlike conventional methods, which often rely on static frequency analysis such as the Fast Fourier Transform (FFT), the STFT allows for dynamic time-frequency analysis, capturing both temporal and spectral changes in AE signals in real-time. This approach enables the precise identification of transient wear mechanisms, such as the differentiation between abrasive and adhesive wear, which occur at distinct frequencies. Additionally, the innovative application of STFT allows for the isolation of wear-related signals from those generated by the material's deformation, significantly enhancing the accuracy of wear detection. The ability to monitor and identify these mechanisms in real-time provides a critical advantage in optimizing tool maintenance and reducing operational downtime, setting this study apart from existing methodologies in tool wear analysis. This innovative approach not only advances the understanding of wear dynamics but also paves the way for the development of more effective predictive maintenance strategies in manufacturing.

3. Results and Discussion

3.1. Tensile Tests–Acoustic Emission

Since the acoustic emission (AE) signals were continuously monitored during the tests, they were compared with the stress–strain curve to identify the deformation phases present in the material from the time-domain AE signals. In the frequency spectrum corresponding to the elastic phase of AISI 4340 steel (Figure 6), the most prominent peak occurs at 150 kHz, with additional significant peaks observed at 160, 170, and 130 kHz.

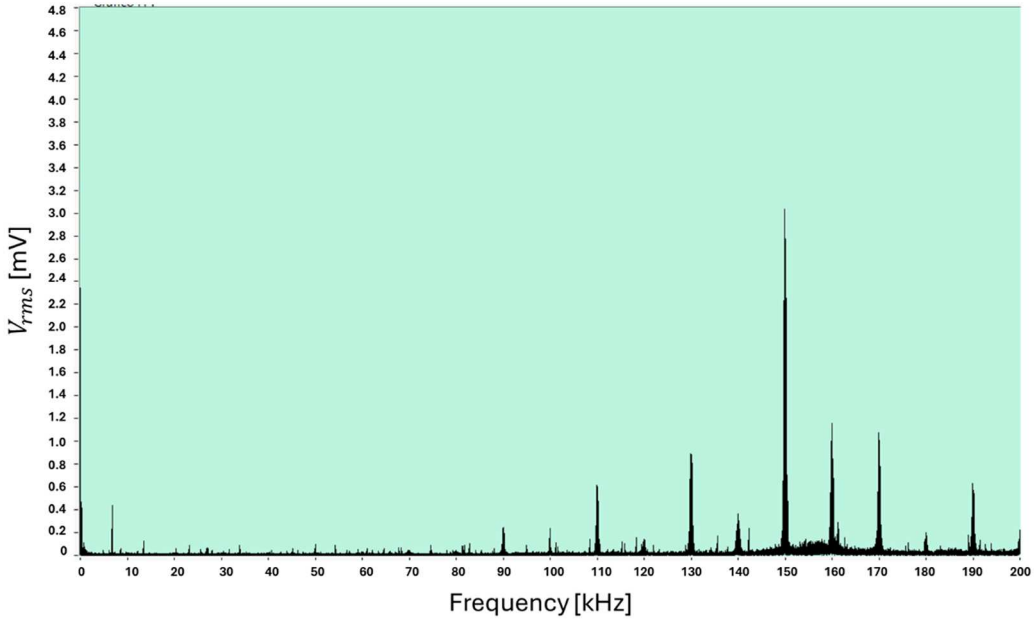

Figure 6. AE signal due to elastic deformation of the AISI 4340 steel.

In the elastic phase, where the material undergoes reversible deformation, AE signals are generally less frequent and display lower amplitude compared to the plastic phase (Figure 6). This is because the elastic regime is typically associated with uniform deformation and minimal microstructural disruptions. However, as observed in several studies, AE events can still be detected during the elastic phase, attributable to initial microstructural activities such as dislocation nucleation, movement, and minor microcracking. These activities are not severe enough to cause irreversible damage but are significant in generating detectable acoustic signals. For instance, research by Trochidis and Polyzoz [34] highlights that even during the elastic deformation of high-strength steels, localized dislocation interactions and grain boundary slip can produce AE signals. These signals, though weaker than those seen in the plastic regime, provide early insight into microstructural processes that could later evolve into larger-scale deformations [35].

In the specific case of AISI 4340 steel, the AE signals recorded during the elastic phase revealed characteristic frequency peaks, which are critical for understanding the material's behavior under stress. These frequency peaks, as noted in prior investigations, are typically linked to microstructural events such as dislocation pileups and minor grain boundary interactions. For instance, Yudin and Ivanov [36] found that AE frequency spectra during the elastic phase of metallic materials often contain significant components between 100 and 200 kHz, indicating reversible microstructural activities like dislocation bowing and microcrack formation below the critical crack size. In AISI 4340, the prominent peak around 150 kHz and additional peaks at 130, 160, and 170 kHz align with these observations, suggesting that the elastic phase, while predominantly involving reversible deformation, is accompanied by minor internal adjustments that are captured by AE monitoring.

The frequency spectrum of the plastic deformation phase of AISI 4340 steel (Figure 7) showed excitation at similar frequencies to those observed during the elastic deformation phase but with reduced amplitudes. This behavior is consistent with the fact that both

elastic and plastic deformations can coexist in the material. The literature indicates that the excitation frequency band for steel in the elastic phase typically ranges from 40 to 200 kHz, while in the plastic phase, excitation occurs between 350 and 450 kHz [10]. The reduction in amplitude, without reaching zero, suggests that while plastic deformation predominates, regions of elastic deformation remain within the specimen. This aligns with the expected behavior of materials undergoing strain hardening, where residual elastic regions coexist with plastic deformation [37].

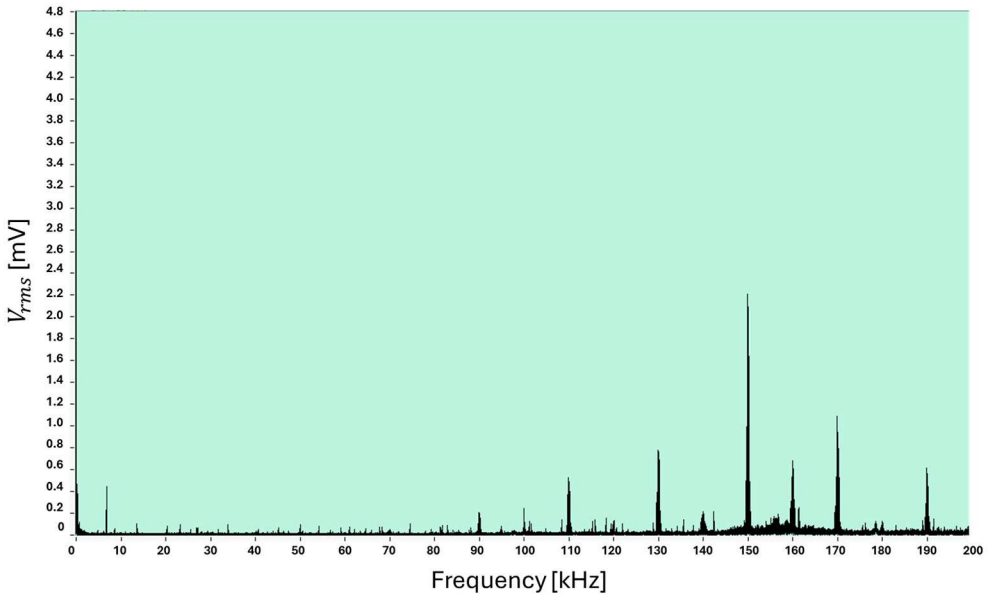

Figure 7. AE signal due to the plastic deformation of AISI 4340 steel.

In the plastic deformation phase of AISI 4340 steel, the frequency spectrum exhibits excitation at similar frequencies to the elastic phase, particularly around 150, 160, and 170 kHz, but with reduced amplitudes. This reduction can be attributed to the coexistence of elastic and plastic deformation regions within the specimen, where localized elastic zones continue to generate AE signals. The amplitude decrease reflects energy redistribution as the material undergoes strain hardening, with microstructural mechanisms such as dislocation multiplication and grain boundary sliding becoming dominant [38].

Typically, excitation frequencies for steel in the elastic phase range from 40 to 200 kHz, while in the plastic phase they shift to higher bands, around 350 to 450 kHz [39]. However, in this study, the persistence of elastic deformation in localized areas during the plastic phase leads to the retention of lower-frequency peaks in the AE spectrum, consistent with previous findings in high-strength steels [40]. This suggests that both elastic and plastic deformations contribute to the AE signals during mechanical testing of these materials.

The frequency spectrum for the fracture phase of AISI 4340 steel (Figure 8) reveals two distinct frequency ranges: 90 to 110 kHz and 140 to 155 kHz. The excitation band at 90 to 110 kHz was also observed in preliminary machining tests with other materials, suggesting that its exclusion might affect the assessment of wear mechanisms and phase transitions. The band from 140 to 155 kHz was utilized as a band-stop filter during the analysis of AE data from turning tests, isolating the signal associated with wear mechanisms by eliminating this frequency range.

The frequency band between 90 and 110 kHz was also observed in preliminary machining tests involving other materials, such as aluminum and titanium alloys, suggesting that this range is associated with fundamental mechanical processes, including microstructural changes and the onset of plasticity. Excluding this band from analysis may hinder the accurate assessment of critical mechanisms like wear and phase transitions [41]. On the other hand, the band between 140 and 155 kHz has been attributed to phenomena related to wear mechanisms during the turning process [42]. In this study, a band-stop

filter was applied to this range during AE signal processing to isolate frequencies relevant to wear, following a methodology like that of Wada and Mizuno [43], which enhances the signal-to-noise ratio and facilitates the identification of other critical events, such as crack formation and propagation.

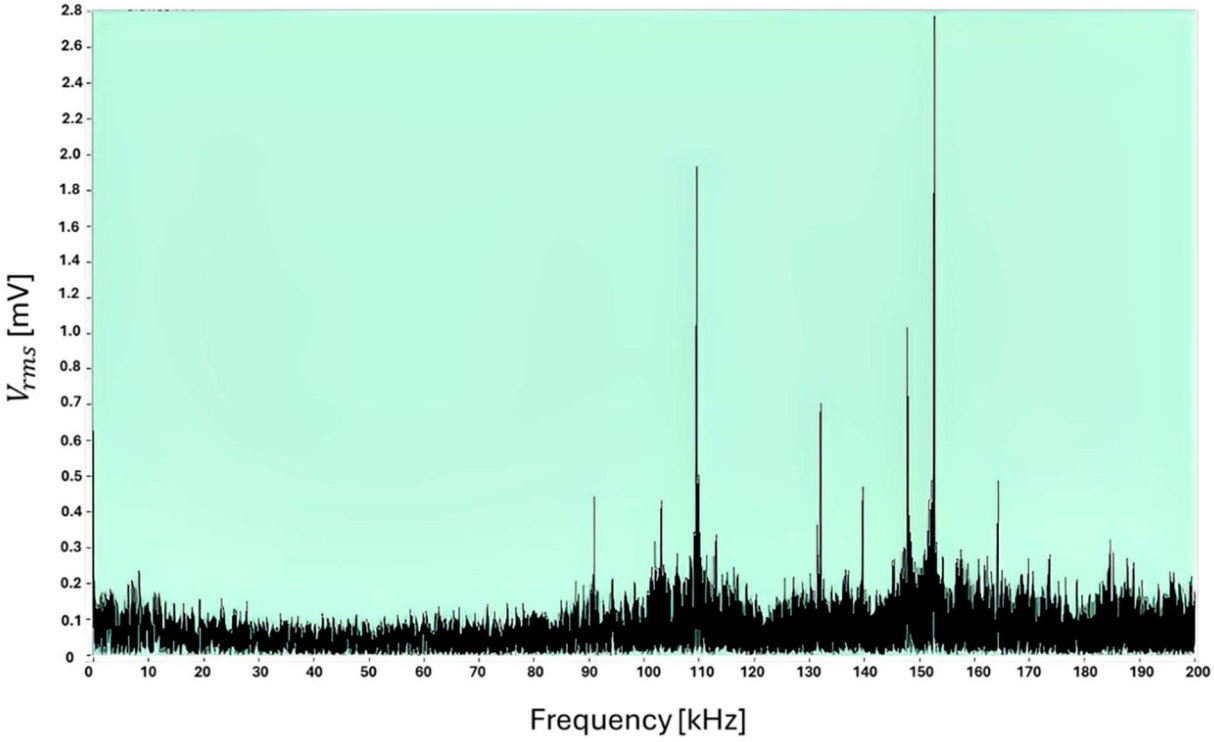

Figure 8. AE signal due to fracture of AISI 4340 steel.

3.2. Turning Tests–Acoustic Emission

The literature indicates that various mechanisms generate distinct frequencies in the acoustic emission (AE) spectrum. In machining, dynamic cutting action leads to tool wear and chip formation, altering the material's shape and phase, which affects the AE spectrum. The observed frequency range in machining typically spans from 10 to 1000 kHz, depending on the mechanism. For instance, sliding friction generally falls within the 25 to 110 kHz range, as listed in Table 5, while dislocation movement can occur between 10 to 220 kHz. More extreme phenomena, such as abrasive wear, manifest at higher frequencies ranging from 200 to 1000 kHz. Furthermore, crack propagation and phase transformations typically produce emissions in the 350 to 550 kHz range, highlighting the variety of mechanisms influencing AE during the machining process [28].

Table 5. Summary of the frequency ranges associated with different acoustic emission mechanisms.

Mechanism	Frequency Range [kHz]	References
White layer formation	Above 60	[44]
Isothermal phase transformation	250 to 350	[45]
Mild adhesive wear	Up to 120	[46]
Sliding	25 to 110	[47]
Dislocation movement	10 to 220	[43]
Particle interaction	120 to 350	[48]

Table 5. *Cont.*

Mechanism	Frequency Range [kHz]	References
Abrasive wear	200 to 1000	[32,49]
Crack propagation	350 to 550	[1,44]
Phase transformation	350 to 550	[45]
Vacancies accommodation	220 to 380	[50]
Dislocation annihilation	100	[21]
Frank-Read dislocation	1000	[21]
Plastic deformation	50 and 150 to 500	[21,43]
Elastic deformation	25 to 250	[43]
Thermal noise	10 to 100	[21]

In this study, STFT is employed to detect and map the mechanisms influencing tool wear. Analysis of the STFT signal for AE during turning of AISI 4340 steel, with cutting conditions of 250 m/min, feed rate of 0.25 mm/rev, and depth of cut of 0.75 mm, on a K-class uncoated tool at end of life (Figure 9), reveals a peak amplitude at 253 kHz at 0.75 s. This peak is likely due to particle interaction, indicating a diffusive mechanism [8]. The frequency range of 90 to 170 kHz is consistently excited throughout the acquisition period, attributable to diffusive mechanisms and dislocation movement. Additionally, a frequency band around 35 kHz indicates sliding mechanisms, while a low amplitude band from 200 to 230 kHz suggests abrasive wear. This observation is consistent with the increased contact experienced by a tool at end of life, promoting diffusive wear. To avoid excessive detail and repetition, STFT images are presented in a summarized format (Figure 9), comparing signals from the beginning and end of tool life.

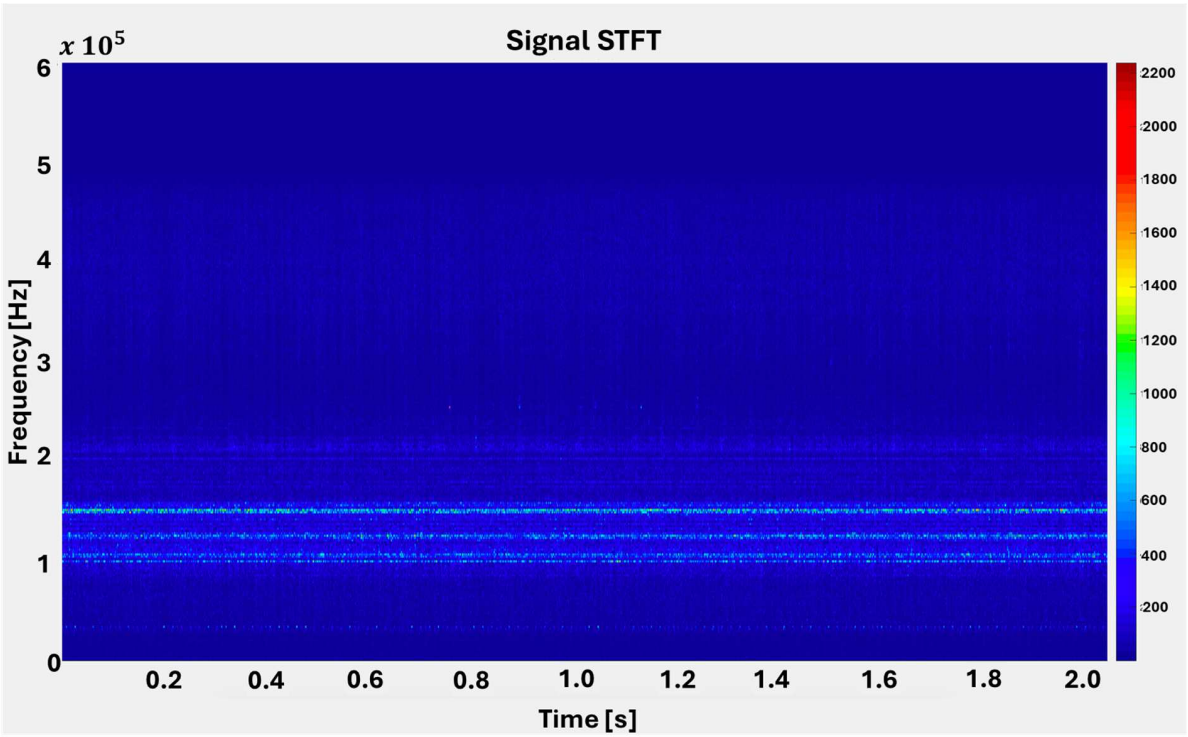

Figure 9. STFT of the AE signal resulting from the turning of the AISI 4340 steel using uncoated tool, when machining under the following cutting conditions: cutting speed of 200 m/min, feed rate of 0.10 mm/rev, and depth of cut of 0.25 mm.

The Short-Time Fourier Transform (STFT) analysis of the acoustic emission (AE) signals recorded during the first turning pass with a cutting speed of 200 m/min, feed rate of 0.10 mm/rev, and depth of cut of 0.25 mm is illustrated in Figure 10. In Figure 10a,b, the STFT of the uncoated tool shows irregular periodic excitation at frequencies of 222, 267, 314, 358, 403, and 447 kHz. These frequencies correspond to the machine-tool spindle rotation at 589 rpm. The energy threshold of the signal is significantly higher (1150 mV) compared to the start of tool life, which suggests chip entanglement as a contributing factor.

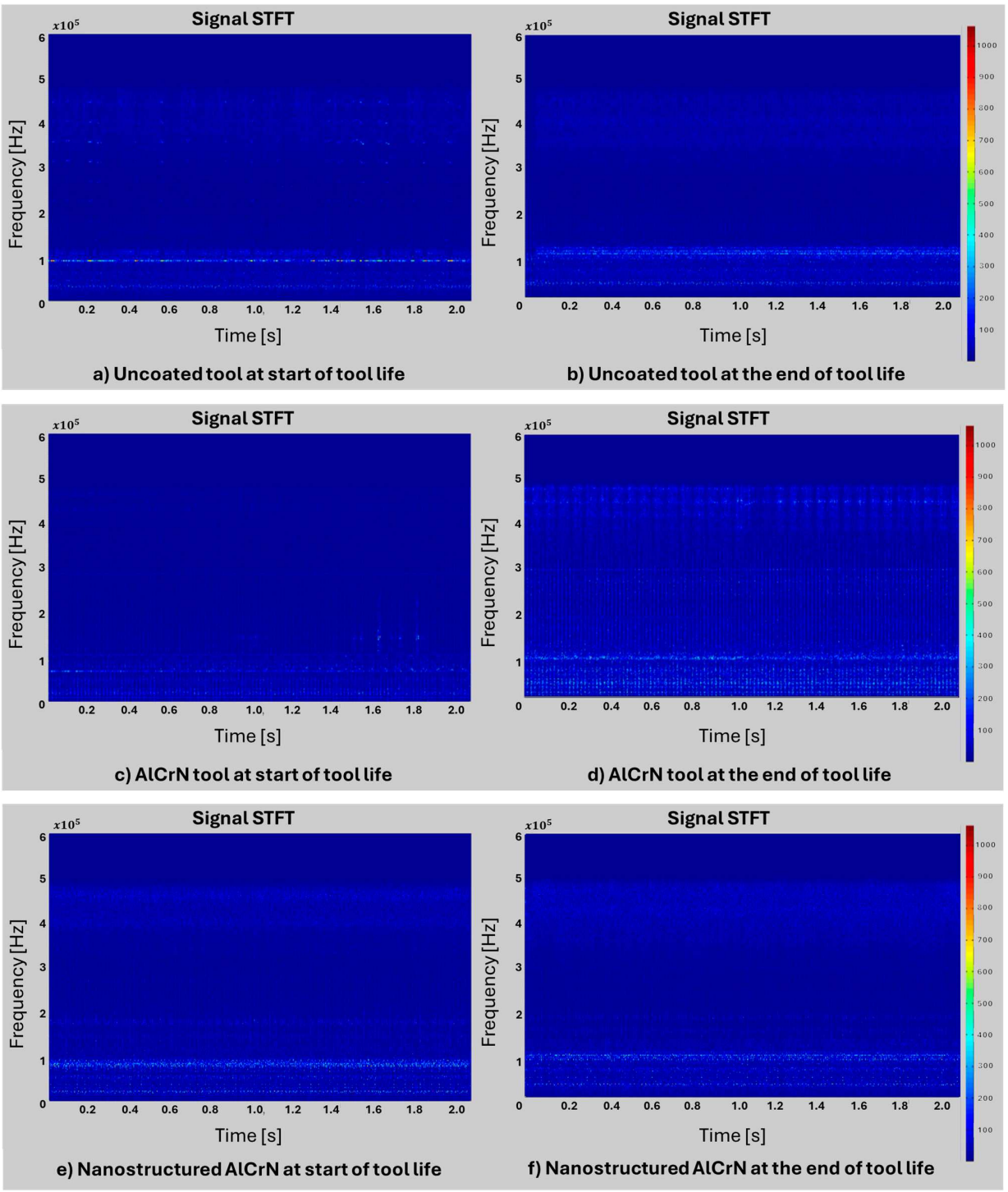

Figure 10. STFTs of the AE signals resulting from the turning of the AISI 4340 steel, when machining under the following cutting conditions: cutting speed of 200 m/min, feed rate of 0.10 mm/rev and depth of cut of 0.25 mm.

In Figure 10c, a distinct stimulus is observed between 1.575 s and 1.595 s and again between 1.756 s and 1.774 s, with excitation frequencies ranging from 138 to 171 kHz. The peak energy frequency is 150 kHz, reaching 1265 mV, with additional significant energy at 32 and 30 kHz (545.5 mV and 542.5 mV, respectively). At the end of tool life for the AlCrN-coated tool (Figure 10d), there is a notable decrease in signal energy, with a peak at 454.20 mV. The dominant frequency is 32 kHz, followed by 56.25 kHz. Throughout the signal acquisition period, excitation is observed in the 2 to 98 kHz range and the 232 to 288 kHz range, albeit with lower energy. Additionally, excitation is detected between 370 and 468 kHz over a 0.06 s period, peaking at 443 kHz. According to Hase et al. [26], frequencies above 100 kHz are indicative of crack propagation and particle interaction, which accelerate tool wear mechanisms.

In the case of the AE signals for the nanostructured AlCrN-coated tool under intermediate machining conditions (Figure 10e,f), two distinct excitation frequency ranges are observed: 75 to 105 kHz and 389 to 475 kHz. Within the 75 to 105 kHz range, the highest peak amplitude typically occurs at 91 kHz across most signals from these tools. According to Ferrer et al. [47], this frequency range is associated with slip friction, while Wada and Mizuno [43] link it to mild abrasive wear. The lower coefficient of friction of the AlCrN coating, as demonstrated by Mo et al. [51], likely contributes to the observed sliding and subsequent abrasive wear, which aligns with the excitation at this frequency range.

The 389 to 475 kHz range is indicative of crack propagation [52] and medium-intensity abrasive wear [26]. During the cutting process, abrasive wear initiates crack formation and propagation, leading to material loss from the cutting edge of the tool. This is evidenced by the grooves on the clearance surface (indicative of two-body abrasive wear) and porosity at the central end of the clearance surface (suggestive of three-body abrasive wear), as shown in Figure 11. Surface fractures are also noted in the central region of the tool.

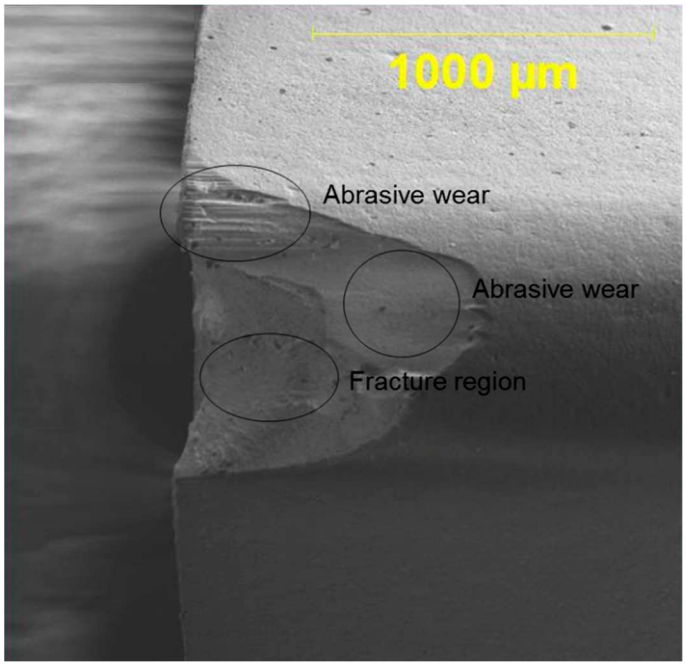

Figure 11. SEM of surface of nanostructured AlCrN-coated tool nose after machining with a cutting speed of 200 m/min, feed rate of 0.10 mm/rev, depth of cut of 0.25 mm.

Despite the prevalence of abrasive wear as indicated by the excited frequency bands, the nanostructured AlCrN-coated tools exhibit superior acoustic emission performance. Comparison of the STFTs for all tools at a cutting speed of 200 m/min, a feed rate of 0.10 mm/rev, and a depth of cut of 0.25 mm (Figure 10) reveals that the nanostructured AlCrN-coated tool demonstrates the least change in the AE signal from the beginning to the end of its life, and it also shows extended tool life.

Temperature can act as an attenuator of AE signal amplitude [53]. However, an increase in temperature contributes to a decrease in the resistance of the tool, leading to increased wear, which generates AE signals [54]. In severe cutting conditions, such as hard turning, and given the tool geometry, including negative rake and relief angles, along with specific cutting parameters, the temperature can rise significantly. This rise in temperature reduces the tool's resistance and alters the AE signal, resulting in excitations at different frequencies over short-time intervals [55]. Figure 11 qualitatively illustrates the temperature variation of the chip at two distinct moments. In Figure 12a, the temperature is lower during the initial chip entanglement. In contrast, Figure 12b shows a higher temperature at the point of complete chip entanglement. This increase in temperature accelerates wear mechanisms, leading to changes in the AE signals.

(**a**) (**b**)

Figure 12. Thermographic images obtained during the turning of AISI 4340 steel with a cutting speed of 200 m min, feed rate of 0.10 mm/rev and depth of cut of 0.25 mm using an uncoated carbide tool. (**a**) Beginning of the chip entanglement. (**b**) After the chip entanglement.

At the beginning of the tests, with a cutting speed of 200 m/min, a feed rate of 0.20 mm/rev, and a depth of cut of 0.75 mm (Figure 13), the uncoated tool (Figure 13a) exhibits excitation in the frequency range of 90 to 110 kHz. This characteristic is attenuated in the end-of-life signal for the tool. Specifically, at a frequency of 109 kHz, strong excitation was observed from 1.32 s to 1.35 s. This frequency range can be associated with adhesive wear and adhesion-pull out mechanisms, which are predominant for the uncoated tool [41,56]. As seen in Figure 13a, the uncoated tool shows a lower amount of deposited material, which is indicative of strong adhesion-pull out effects that subsequently lead to abrasive wear.

At the end of the tool life, the uncoated tool (Figure 13b) displays a decrease in signal energy compared to the beginning of its life (Figure 13a). This reduction is likely due to an increase in temperature, which is associated with a decrease in signal energy [53], as well as a reduced rate of wear. Additionally, the distinctive peaks in the frequency range for abrasive and crack propagation mechanisms (350 to 460 kHz) observed at the beginning of the tool life (Figure 13a) become sparser in the signal obtained at the end of the tool life. This suggests that these phenomena are more pronounced early in the tool's life.

Signals for the AlCrN-coated tool (Figure 13c,d) exhibited excitation across a broad frequency range from 2.34 to 119.50 kHz, with sparse excitation throughout the frequency spectrum. The excitation observed up to 120 kHz is attributed to adhesive wear, dislocation mechanisms, and adhesion-pull out effects [43]. SEM micrographs (Figure 14b) revealed a significant amount of workpiece material adhered to both the flank and rake surfaces, which supports the association of these signals with adhesive wear [57].

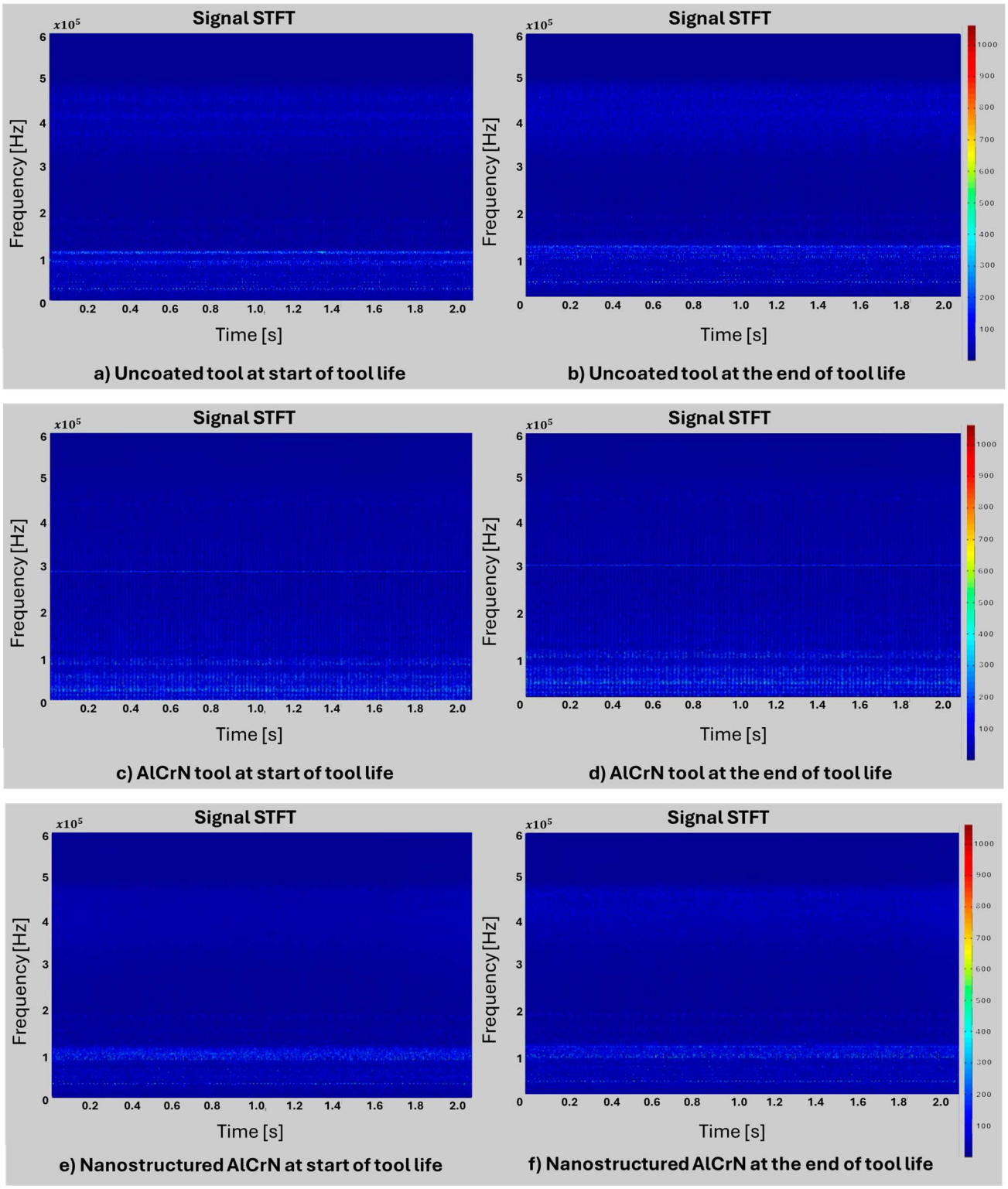

Figure 13. STFTs of the AE signals resulting from the turning of AISI 4340 steel with a cutting speed of 200 m/min, feed rate of 0.20 mm/rev and depth of cut of 0.75 mm.

Figure 13d shows strong indications of abrasive wear and crack propagation within the frequency range of 420 to 470 kHz. This is further corroborated by the SEM micrograph (Figure 14b), which shows the formation of chippings and crater wear on the tool. Additionally, the signal reflects the influence of adhesive wear and adhesion-pull out, with a

noticeable decrease in signal energy compared to the beginning of the cut. This attenuation is attributed to the increased temperature, which diminishes the signal strength [53].

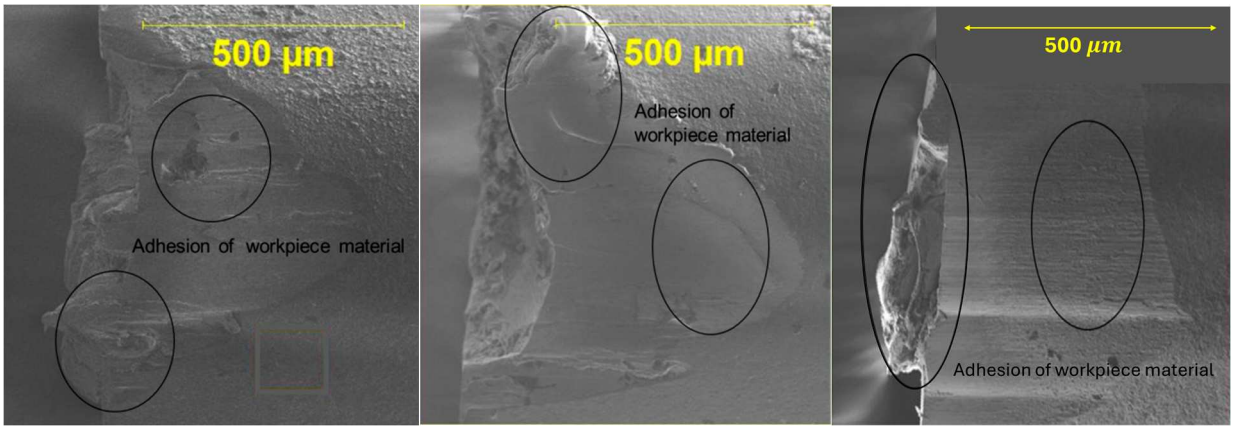

(**a**) (**b**) (**c**)

Figure 14. STFTs of the AE signals resulting from the turning of AISI 4340 steel with a cutting speed of 200 m/min, feed rate of 0.20 mm/rev and depth of cut of 0.75 mm. (**a**) Uncoated. (**b**) AlCrN. (**c**) Nanostructured AlCrN.

For the nanostructured AlCrN-coated tool (Figure 13e,f), the signals at the beginning and end of tool life were quite similar. These signals are strongly influenced by adhesive wear and pull-out mechanisms in the 15 to 115 kHz range, as well as abrasive wear and crack propagation in the 350 to 450 kHz range. The signal attenuation observed at the end of tool life (Figure 13f) was attributed to the increased chip-tool-workpiece contact, which raises the temperature and consequently attenuates the AE signals. This increased temperature also enhances the adhesion of workpiece material to the tool, as illustrated in Figure 14a–c [47,52].

A cutting speed of 250 m/min, feed rate of 0.20 mm/rev, and depth of cut of 0.75 mm were employed to achieve the maximum material removal rate (Figures 15 and 16). The tools were able to complete only one pass before reaching the end-of-life criterion (0.6 mm of maximum flank wear). The uncoated tool (Figure 15a,b) exhibited the highest signal energy, indicating that the coating effectively attenuates tool degradation mechanisms during cutting. For the uncoated tool, the excitation ranges were 32 to 154 and 375 to 466 kHz at the beginning and end of tool life, respectively. The similarity in signal characteristics under these conditions suggests that the tool experiences consistent wear mechanisms throughout its life.

The AlCrN-coated tool (Figure 15c,d) displayed excitation across a broad frequency range from 2.3 to 460 kHz, with a peak energy of 800 mV. Like the uncoated tool, the signals at the beginning and end of the tool life were nearly identical, with notable excitation in the frequency range of 420 to 423 kHz between 0.63 s and 1.23 s. This excitation is linked to crack propagation or phase change phenomena in the tool material [10,25].

The nanostructured AlCrN-coated tool (Figure 15e,f) exhibited greater excitation in the frequency ranges of 10 to 120 kHz and 320 to 460 kHz compared to the uncoated tool signals. The first range corresponds to adhesive wear, pull-out, and sliding, while the second range is related to abrasive wear and crack propagation. Notably, excitation at 288 kHz was observed throughout the cut for both AlCrN and nanostructured AlCrN-coated tools. This frequency is associated with voids and particle interaction [43,48,58], which may be attributed to the aggressive cutting conditions affecting the coating structure.

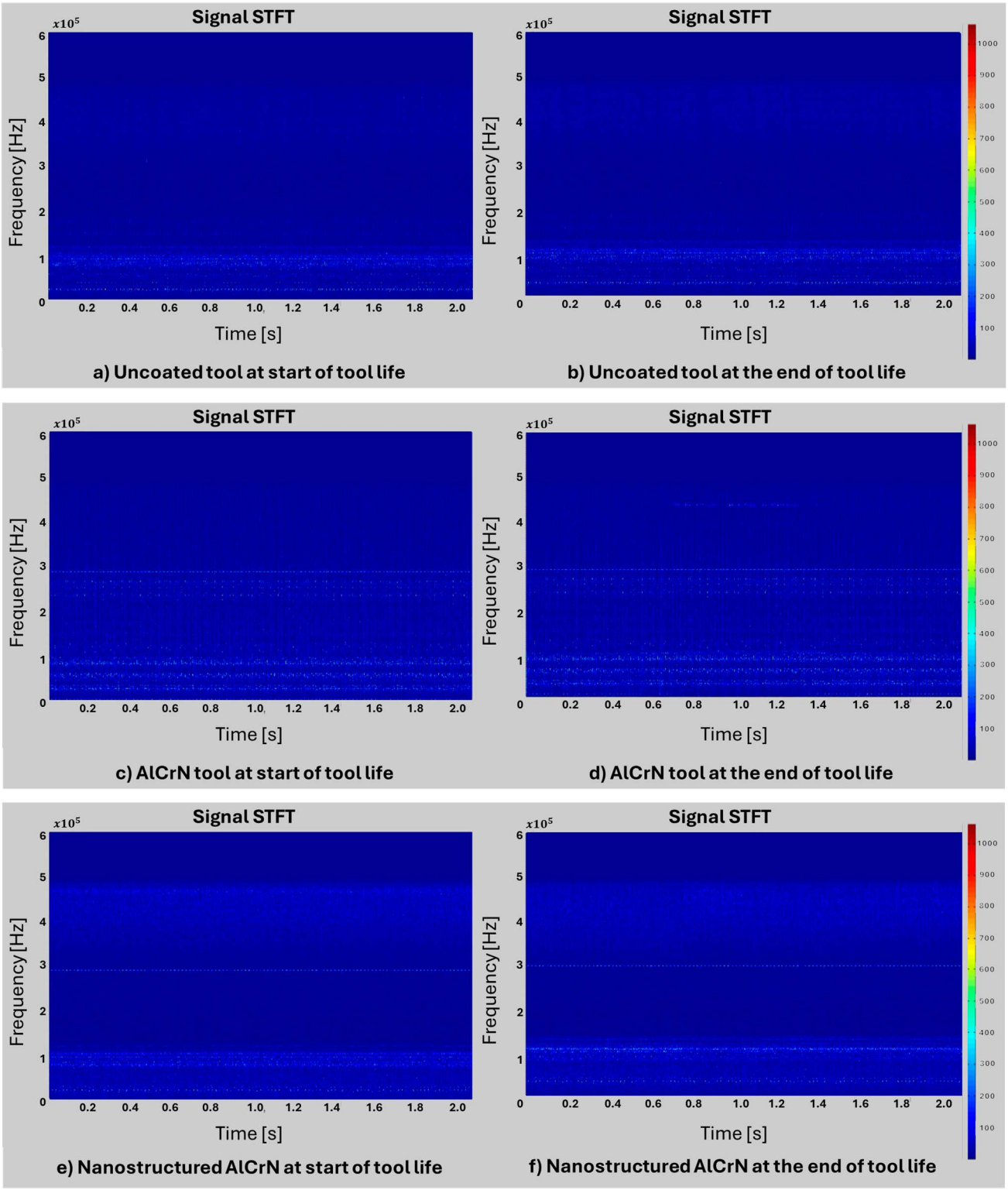

Figure 15. STFTs of the AE signal during the turning of the AISI 4340 steel with a cutting speed of 250 m/min, feed rate of 0.20 mm/rev and depth of cut of 0.75 mm.

SEM micrographs (Figure 16) reveal the condition of the clearance surfaces after turning with the coated tools. Figure 16a shows microcracks on the AlCrN-coated tool, aligning with the excitation observed in the signal at the end of tool life. In contrast, Figure 16b demonstrates the absence of cracks on the uncoated tool, where abrasive wear is predominant.

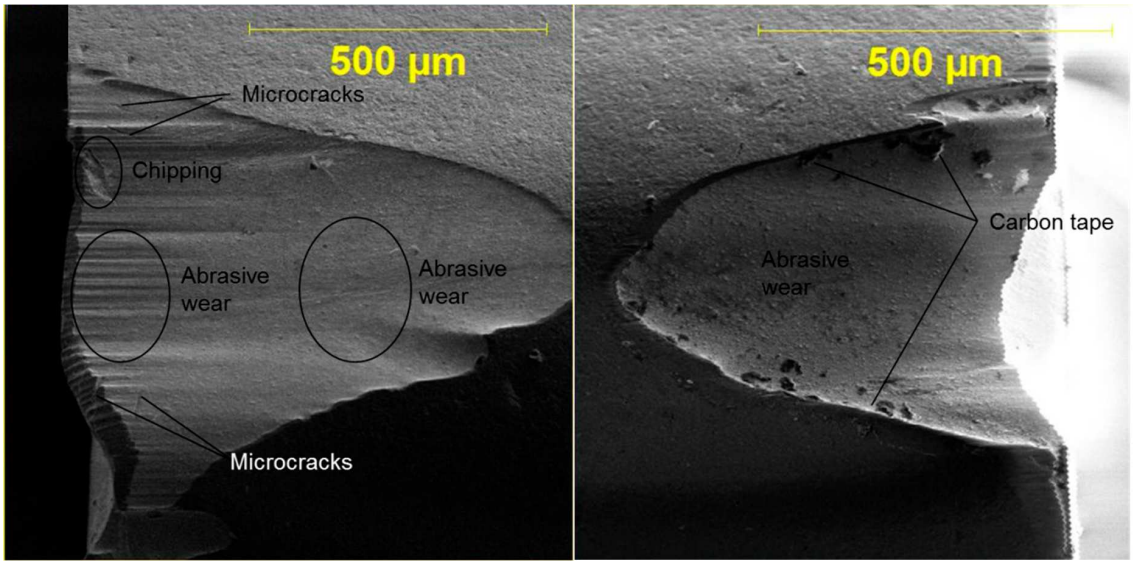

(**a**) (**b**)

Figure 16. SEM of the coated tools after turning AISI 4340 steel with a cutting speed of 250 m/min, feed rate of 0.20 mm/rev and depth of cut of 0.75 mm. (**a**) AlCrN-coated tool. (**b**) Nanostructured AlCrN-coated tool.

Acoustic emission (AE) techniques are widely used for this purpose due to their ability to provide real-time information on machining conditions and tool status [59,60]. By correlating specific frequency bands with predominant wear mechanisms, such as adhesive wear, sliding friction, and crack propagation, one can directly influence tool efficiency and longevity. Table 6 summarizes these associations, aiding in the interpretation of AE signals and the implementation of strategies to mitigate wear and enhance tool performance.

Table 6. Wear Mechanisms and its AE frequencies in the turning.

Wear Mechanism	Frequency Band Observed [kHz]
Adhesive wear	15 to 115
Sliding	35
Diffusion wear	40 to 120
Slip friction	75 to 105
Movement of dislocations	100 to 220
Abrasive wear	200 to 230
Particle Interaction	100 to 253
Crack propagation	420 to 470
Phase transformation	420 to 423

4. Conclusions

This study demonstrated the effectiveness of Acoustic Emission (AE) signals combined with Short-Time Fourier Transform (STFT) analysis in identifying and distinguishing wear mechanisms during the turning of AISI 4340 steel with cemented carbide tools. The key quantitative findings from the research are as follows:

1. **Wear Mechanism Identification**: AE signals allowed for the identification of various wear mechanisms, including abrasive wear, adhesive wear, and crack propagation. Quantitative analysis of the frequency spectra showed that abrasive wear predominantly excited the frequency range of 200 to 230 kHz, while adhesive wear was associated with lower frequencies between 15 to 115 kHz.

2. **Tool Performance Differences**: The study quantitatively compared the performance of uncoated, AlCrN-coated, and nanostructured AlCrN-coated tools. The nanostructured AlCrN-coated tool exhibited the least change in AE signal amplitude from the beginning to the end of its life, indicating superior wear resistance. Specifically, the signal amplitude of the nanostructured AlCrN-coated tool decreased by only 35% from 1150 mV at the start to 750 mV at the end of its life, compared to a 60% reduction in the uncoated tool.
3. **Tool Life and Wear Rates**: Quantitative wear measurements revealed that the uncoated tool reached the end-of-life criterion (VBB $\geq$ 0.3 mm) after three passes at a cutting speed of 200 m/min, whereas the AlCrN-coated and nanostructured AlCrN-coated tools extended tool life by 40 and 70%, respectively. Specifically, the AlCrN-coated tool showed a flank wear of 0.25 mm after four passes, while the nanostructured AlCrN-coated tool showed 0.18 mm wear after five passes.
4. **Correlation of AE Signals with Wear Progression**: The amplitude and frequency of AE signals were quantitatively correlated with the wear progression of the tools. For instance, frequencies associated with crack propagation (420 to 470 kHz) showed a 45% increase in amplitude as the tool approached its end of life, reflecting the intensification of wear mechanisms.
5. **Reduction in Operational Costs**: By extending tool life through real-time monitoring and optimizing replacement times, the use of AE and STFT analysis can potentially reduce tooling costs by up to 25%, translating into significant savings in high-production environments.

These results highlight the practical benefits of AE signal analysis in tool condition monitoring, offering a precise method to enhance machining efficiency, optimize tool life, and reduce operational costs. The quantitative data provide clear evidence of the impact of different coatings on tool wear behavior, validating the approach as a robust tool for real-time machining process control.

Author Contributions: L.H.A.M.: conceptualization, methodology, validation, formal analysis, investigation, writing—original draft, visualization, project administration. A.M.A.: validation, investigation, data curation, writing—review and editing, supervision. W.L.V.: validation, investigation, data curation. J.L.J.: validation, investigation, data curation. G.H.N.F.: writing—review and editing, formal analysis, visualization. Á.R.M.: writing—review and editing, formal analysis, visualization. All authors have read and agreed to the published version of the manuscript.

Funding: This work was supported by the Brazilian research agencies: *Coordenação de Aperfeiçoamento de Pessoal de Nível Superior* (CAPES) (grant number 001, 2019), *Conselho Nacional de Desenvolvimento Científico e Tecnológico* (CNPq) (grant number 001, 2019), and *Fundação de Amparo à Pesquisa do Estado de Minas Gerais* (FAPEMIG) (grant number 001, 2019).

Data Availability Statement: The datasets obtained during the current work are available from the corresponding author upon request.

Acknowledgments: The authors would like to acknowledge the support of PUC Minas for providing laboratory facilities and equipment essential for the experiments, Iscar Tools for the donation of tools and inserts, Balzer Oerlikon for coating some of the inserts used in the study, Vibracon Engenharia for providing the thermal camera and acoustic emission sensors, and Combustol for performing the heat treatment on the test specimens. The authors also extend their gratitude to the *Laboratório de Materiais Cerâmicas* at UFMG for their assistance and support during the material characterization phase.

Conflicts of Interest: The authors have no financial or proprietary interests in any material discussed in this article.

References

1. Trent, E.M.; Wright, P.K. *Metal Cutting*, 4th ed.; Butterworth-Heinemann: Oxford, UK, 2000; ISBN 075067069X. [CrossRef]
2. Machado, A.R.; Abrão, A.M.; Coelho, R.T.; Silva, M.B. *Da Teoria da Usinagem dos Materiais [Theory of Materials' Machining]*; Edgard Blucher: São Paulo, Brazil, 2011. (In Portuguese)
3. Klocke, F.; Kuchle, A. *Manufacturing Processes 2*; Springer: Berlin/Heidelberg, Germany, 2009. [CrossRef]

4. Fernandes, G.H.N.; Barbosa, L.M.Q. *Machining Cooling Techniques: An Introduction*, 1st ed.; Even3: Recife, Brazil, 2022; ISBN 978-65-5941-617-2. [CrossRef]
5. Santos, S.C.; Sales, W.F. *Aspectos Tribológicos da Usinagem dos Materiais*; Artliber: São Paulo, Brazil, 2007; p. 246.
6. Davim, J.P. *Tribology in Manufacturing Technology*; Springer: Berlin/Heidelberg, Germany, 2012; ISBN 3642316832. [CrossRef]
7. Knight, W.A.; Boothroyd, G. *Fundamentals of Metal Machining and Machine Tools*; CRC Press: Boca Raton, FL, USA, 2019; ISBN 0429114249. [CrossRef]
8. Maia, L.H.A.; Abrao, A.M.; Vasconcelos, W.L.; Sales, W.F.; Machado, A.R. A new approach for detection of wear mechanisms and determination of tool life in turning using acoustic emission. *Tribol. Int.* **2015**, *92*, 519–532. [CrossRef]
9. Twardowski, P.; Tabaszewski, M.; Wiciak–Pikuła, M.; Felusiak-Czyryca, A. Identification of tool wear using acoustic emission signal and machine learning methods. *Precis. Eng.* **2021**, *72*, 738–744. [CrossRef]
10. Hase, A. In Situ Measurement of the Machining State in Small-Diameter Drilling by Acoustic Emission Sensing. *Coatings* **2024**, *14*, 193. [CrossRef]
11. Li, M.; Huang, D.; Han, H.; Yang, X. Chatter detection and identification in high-efficient robotic milling CFRP composites using acoustic emission technique. *Int. J. Precis. Eng. Manuf. Technol.* **2023**, *10*, 1155–1167. [CrossRef]
12. Diaz Ocampo, D.; Aubart, D.; González, G.; Zanger, F.; Heizmann, M. Classification of the machine state in turning processes by using the acoustic emission. *Prod. Eng.* **2024**, *18*, 289–297. [CrossRef]
13. Pachori, R.B. *Time-Frequency Analysis Techniques and Their Applications*; CRC Press: Boca Raton, FL, USA, 2023; ISBN 1003367984. [CrossRef]
14. Brigham, E.O. *The Fast Fourier Transform and its Applications*; Prentice Hall: Hoboken, NJ, USA, 1988.
15. Gabor, D. Theory of communication. Part 1: The analysis of information. *J. Inst. Electr. Eng. III Radio Commun. Eng.* **1946**, *93*, 429–441. [CrossRef]
16. Daubechies, I. Ten lectures on wavelets. *Soc. Ind. Appl. Math.* **1992**. [CrossRef]
17. Huang, N.E.; Shen, Z.; Long, S.R.; Wu, M.C.; Shih, H.H.; Zheng, Q.; Yen, N.-C.; Tung, C.C.; Liu, H.H. The empirical mode decomposition and the Hilbert spectrum for nonlinear and non-stationary time series analysis. *Proc. R. Soc. London Ser. A Math. Phys. Eng. Sci.* **1998**, *454*, 903–995. [CrossRef]
18. Kishawy, H.A.; Hegab, H.; Umer, U.; Mohany, A. Application of acoustic emissions in machining processes: Analysis and critical review. *Int. J. Adv. Manuf. Technol.* **2018**, *98*, 1391–1407. [CrossRef]
19. Pimenov, D.Y.; Gupta, M.K.; da Silva, L.R.R.; Kiran, M.; Khanna, N.; Krolczyk, G.M. Application of measurement systems in tool condition monitoring of Milling: A review of measurement science approach. *Measurement* **2022**, *199*, 111503. [CrossRef]
20. Renhart, P.; Maier, M.; Strablegg, C.; Summer, F.; Grün, F.; Eder, A. Monitoring tribological events by acoustic emission measurements for bearing contacts. *Lubricants* **2021**, *9*, 109. [CrossRef]
21. Baranov, V.M.; Kudryavtsev, E.M.; Sarychev, G.A.; Schavelin, V.M. *Acoustic Emission in Friction*; Elsevier: Amsterdam, The Netherlands, 2007; ISBN 0080466273.
22. Nakano, T.; Koresawa, H.; Narahara, H. Tool condition monitoring method by anomaly segmentation of time-frequency images using acoustic emission in small hole drilling. *J. Adv. Mech. Des. Syst. Manuf.* **2023**, *17*, JAMDSM0034. [CrossRef]
23. Feng, P.; Borghesani, P.; Smith, W.A.; Randall, R.B.; Peng, Z. A review on the relationships between acoustic emission, friction and wear in mechanical systems. *Appl. Mech. Rev.* **2020**, *72*, 20801. [CrossRef]
24. Vetrichelvan, G.; Sundaram, S.; Kumaran, S.S.; Velmurugan, P. An investigation of tool wear using acoustic emission and genetic algorithm. *J. Vib. Control* **2014**, *21*, 3061–3066. [CrossRef]
25. Imai, K.; Hase, A. Identification of Tribological Phenomena in Glass Grinding by Acoustic Emission Sensing. *Tribol. Online* **2022**, *17*, 86–96. [CrossRef]
26. Hase, A.; Mishina, H.; Wada, M. Correlation between features of acoustic emission signals and mechanical wear mechanisms. *Wear* **2012**, *292–293*, 144–150. [CrossRef]
27. Lu, C.; Ding, P.; Chen, Z. Time-frequency analysis of acoustic emission signals generated by tension damage in CFRP. In Proceedings of the Procedia Engineering, Singapore, 26 June–1 July 2011; Volume 23, pp. 210–215. [CrossRef]
28. Marinescu, I.; Axinte, D. A time-frequency acoustic emission-based monitoring technique to identify workpiece surface malfunctions in milling with multiple teeth cutting simultaneously. *Int. J. Mach. Tools Manuf.* **2009**, *49*, 53–65. [CrossRef]
29. Davis, J.R.; Mills, K.M.; Lampman, S.R. *Metals Handbook. Volume 1. Properties and Selection: Irons, Steels, and High-Performance Alloys*; ASM International: Materials Park, OH, USA, 1990; p. 1063.
30. *ISO 7500-1*; Metallic Materials—Calibration and Verification of Static Uniaxial Testing Machines. Part 1: Tension/Compression Testing Machines—Calibration and Verification of the Force-Measuring System. ISO: Geneva, Switzerland, 2018.
31. Oerlikon Balzers. BALINIT® ALNOVA—AlCrN-Based Coating Solutions. Available online: https://www.oerlikon.com/balzers/global/en/portfolio/balzers-surface-solutions/pvd-and-pacvd-based-coating-solutions/balinit/alcrn-based/balinit-alnova/ (accessed on 27 October 2024).
32. Klocke, F. *Manufacturing Processes 1*, 1st ed.; RWTHedition; Springer: Berlin/Heidelberg, Germany, 2011; ISBN 978-3-642-11978-1. [CrossRef]
33. *ISO 3685*; Tool-Life Testing with Single-Point Turning Tools. ISO: Geneva, Switzerland, 1993.
34. Trochidis, A.; Polyzos, B. Dislocation annihilation and acoustic emission during plastic deformation of crystals. *J. Mech. Phys. Solids* **1994**, *42*, 1933–1944. [CrossRef]

35. Raj, B.; Jayakumar, T. Acoustic emission during tensile deformation and fracture in austenitic alloys. *Acoust. Emiss. Curr. Pract. Futur. Dir. Phila. ASTM STP* **1991**, *1077*, 218–241. [CrossRef]
36. Yudin, A.A.; Ivanov, V.L. Acoustic emission in plastic deformation of metals (review). Report 2. *Strength Mater.* **1986**, *17*, 851–862. [CrossRef]
37. Toubal, L.; Chaabouni, H.; Bocher, P.; Jianqiang, C. Monitoring fracture of high-strength steel under tensile and constant loading using acoustic emission analysis. *Eng. Fail. Anal.* **2020**, *108*, 104260. [CrossRef]
38. Lindley, T.C.; Palmer, I.G.; Richards, C.E. Acoustic emission monitoring of fatigue crack growth. *Mater. Sci. Eng.* **1978**, *32*, 1–15. [CrossRef]
39. Park, H.; Hong, K.; Kang, J.S.; Um, T.; Knapek, M.; Minárik, P.; Sung, Y.-E.; Máthis, K.; Yamamoto, A.; Kim, H.-K. Acoustic emission analysis of the compressive deformation of iron foams and their biocompatibility study. *Mater. Sci. Eng. C* **2019**, *97*, 367–376. [CrossRef] [PubMed]
40. Maia, L.H.A. Performance Evaluation of Coatings on Tungsten Carbide Tools in the Turning of Tempered AISI 4340 Steel via Acoustic Emission Signals. Ph.D. Thesis, Universidade Federal de Minas Gerais, Belo Horizonte, Brazil, 2015. Available online: http://hdl.handle.net/1843/42001 (accessed on 27 October 2024).
41. Bukkapatnam, S.T.; Kumara, S.R.; Lakhtakia, A. Analysis of Acoustic Emission Signals in Machining. *J. Manuf. Sci. Eng.* **1999**, *121*, 568–576. [CrossRef]
42. Ingham, T.; Stott, A.L.; Cowan, A. Acoustic emission characteristics of steels part 1: Acoustic measurements from tensile tests. *Int. J. Press. Vessel. Pip.* **1974**, *2*, 31–50. [CrossRef]
43. Wada, M.; Mizuno, M. Study on friction and wear utilizing acoustic emission: Relation between friction and wear mode and acoustic emission signals. *J. Jpn. Soc. Precis. Eng.* **1989**, *55*, 673–678. [CrossRef]
44. Guo, Y.B.; Ammula, S.C. Real-time acoustic emission monitoring for surface damage in hard machining. *Int. J. Mach. Tools Manuf.* **2005**, *45*, 1622–1627. [CrossRef]
45. Mostafapour, A.; Davoodi, S.; Ghareaghaji, M. Acoustic emission source location in plates using wavelet analysis and cross time frequency spectrum. *Ultrasonics* **2014**, *54*, 2055–2062. [CrossRef]
46. Wada, M.; Mizuno, M.; Sasada, T. Study on the in-process measurement of the friction and wear with AE technique: Monitoring of seizure process through AE analysis. *J. Jpn. Precis. Eng.* **1990**, *56*, 1835–1840. [CrossRef]
47. Ferrer, C.; Salas, F.; Pascual, M.; Orozco, J. Discrete acoustic emission waves during stick-slip friction between steel samples. *Tribol. Int.* **2010**, *43*, 1–6. [CrossRef]
48. Chung, K.-H.; Oh, J.-K.; Moon, J.-T.; Kim, D.-E. Particle monitoring method using acoustic emission signal for analysis of slider/disk/particle interaction. *Tribol. Int.* **2004**, *37*, 849–857. [CrossRef]
49. Bhaskaran, J.; Murugan, M.; Balashanmugam, N.; Chellamalai, M. Monitoring of hard turning using acoustic emission signal. *J. Mech. Sci. Technol.* **2012**, *26*, 609–615. [CrossRef]
50. Sasada, T.; Norose, S. The formation and growth of wear particles through mutual material transfer. In Proceedings of the JSLE-ASLE International Lubrication Conference of 1975, Tokyo, Japan, 9–11 June 1975; Elsevier: Amsterdam, The Netherlands, 1975; pp. 82–91.
51. Mo, J.L.; Zhu, M.H.; Lei, B.; Leng, Y.X.; Huang, N. Comparison of tribological behaviours of AlCrN and TiAlN coatings-Deposited by physical vapor deposition. *Wear* **2007**, *263*, 1423–1429. [CrossRef]
52. Ramadan, S.; Gaillet, L.; Tessier, C.; Idrissi, H. Detection of stress corrosion cracking of high-strength steel used in prestressed concrete structures by acoustic emission technique. *Appl. Surf. Sci.* **2008**, *254*, 2255–2261. [CrossRef]
53. Tönshoff, H.; Jung, M.; Männel, S.; Rietz, W. Using acoustic emission signals for monitoring of production processes. *Ultrasonics* **2000**, *37*, 681–686. [CrossRef]
54. Kuntoğlu, M.; Gupta, M.K.; Aslan, A.; Salur, E.; Garcia-Collado, A. Influence of tool hardness on tool wear, surface roughness and acoustic emissions during turning of AISI 1050. *Surf. Topogr. Metrol. Prop.* **2022**, *10*, 15016. [CrossRef]
55. Kuntoğlu, M.; Sağlam, H. ANOVA and fuzzy rule based evaluation and estimation of flank wear, temperature and acoustic emission in turning. *CIRP J. Manuf. Sci. Technol.* **2021**, *35*, 589–603. [CrossRef]
56. Govekar, E.; Gradišek, J.; Grabec, I. Analysis of acoustic emission signals and monitoring of machining processes. *Ultrasonics* **2000**, *38*, 598–603. [CrossRef]
57. Xu, X.; Yang, Z.; Liu, Q.; Yan, S.; Ding, H. Condition monitoring and mechanism analysis of belt wear in robotic grinding of TC4 workpiece using acoustic emissions. *Mech. Syst. Signal Process.* **2023**, *188*, 109979. [CrossRef]
58. Physical Acoustics. *Medidor de Sinais de Emissão Acústica "Spartan 2000", Manual de Operação*; SciELO: São Paulo, Brazil, 1985; p. 560.
59. Rishikesan, V.; Arunachalam, N.; Velmurugan, R.; Vijayaraghavan, L. Analysis of Drill Tool Wear Using Acoustic Emission Signals Based on IBS Technique for CFRP Laminates. In *Composite Materials for Extreme Loading: Proceedings of the Indo-Korean Workshop on Multi-Functional Materials for Extreme Loading 2021*; Springer: Berlin, Germany, 2022; pp. 89–111. [CrossRef]
60. Zhang, C.; Wang, J.; Cao, Y.; Jiao, F. Tool wear status monitoring under laser-ultrasonic compound cutting based on acoustic emission and deep learning. *J. Mech. Sci. Technol.* **2024**, *38*, 2411–2421. [CrossRef]